Naval Research Laboratory

Washington, DC 20375-5320

NRL/MR/6750--08-9141

Electron Temperature Derived from Measurements of Complex Plasma Impedance

D. N. Walker

Global Strategies Group Inc.
Crofton, Maryland

R. F. Fernsler
D. D. Blackwell
W. E. Amatucci

Charged Particle Physics Branch
Plasma Physics Division

October 20, 2008

REPORT DOCUMENTATION PAGE

Form Approved OMB No. 0704-0188

1. REPORT DATE *(DD-MM-YYYY)*	2. REPORT TYPE	3. DATES COVERED *(From - To)*
20-10-2008	Memorandum Report	

4. TITLE AND SUBTITLE

Electron Temperature Derived from Measurements of Complex Plasma Impedance

5a. CONTRACT NUMBER

5b. GRANT NUMBER

5c. PROGRAM ELEMENT NUMBER

6. AUTHOR(S)

D. N. Walker*, R. F. Fernsler, D. D. Blackwell, and W. E. Amatucci

5d. PROJECT NUMBER

5e. TASK NUMBER

5f. WORK UNIT NUMBER

7. PERFORMING ORGANIZATION NAME(S) AND ADDRESS(ES)

Naval Research Laboratory
4555 Overlook Avenue, SW
Washington, DC 20375-5320

*Global Strategies Group (North America) Inc.
2200 Defense Highway
Crofton, MD 21114

8. PERFORMING ORGANIZATION REPORT NUMBER

NRL/MR/6750--08-9141

9. SPONSORING / MONITORING AGENCY NAME(S) AND ADDRESS(ES)

Office of Naval Research
Suite 425
875 North Randolf Street
Arlington, VA 22203-1995

10. SPONSOR / MONITOR'S ACRONYM(S)

ONR

11. SPONSOR / MONITOR'S REPORT NUMBER(S)

12. DISTRIBUTION / AVAILABILITY STATEMENT

Approved for public release; distribution is unlimited.

13. SUPPLEMENTARY NOTES

14. ABSTRACT

In earlier work, using a network analyzer, we have shown the existence of collisionless resistance (CR) in the sheath of a spherical probe when driven by a small RF signal. For any position in the sheath, the CR was shown to be inversely proportional to the plasma density gradient there; but to exist only when the applied frequency corresponds to the plasma frequency (ω_{pe}), or density, at that position. We have recently begun a study of the low-to-intermediate frequency response of the probe to the RF signal. At sufficiently low frequencies, the CR is beyond cutoff, i.e., since the earlier work shows that the existence of CR depends on the plasma density gradient, there is a cutoff which is proportional to the applied bias level and which will occur at the plasma frequency at the surface of the probe. Since electron density at the probe surface decreases as a function of applied (negative) bias, the CR will extend to lower frequencies as the magnitude of negative bias increases. Therefore, to eliminate both CR and ion current contributions, the frequencies we consider are much greater than the ion plasma frequency (ω_{pi}), but less than the plasma frequency at the probe surface ($\omega_{pe}(r_0)$), where r_0 is the probe radius. We show that, in this frequency regime, the complex impedance measurements made with a network analyzer can be used to determine electron temperature. We present an overview of the theory used along with comparisons to data sets made using three stainless steel spherical probes of different sizes in different experimental environments and different plasma parameter regimes. We compare the results of the temperature measurements to those made by conventional Langmuir probe sweeps; the method shown here requires no curve fitting as is the usual procedure with Langmuir probes when a Maxwell Boltzmann electron distribution function is assumed. This method requires only a solution of the Poisson equation to determine the approximate sheath dimensions and integrals to determine approximate plasma and sheath inductances. The basis of the solution relies on the calculation of impedance for a spherical probe immersed in a collisionless plasma and appeals to a circuit analogy to solve for electron temperature, T_e, using the experimental data.

15. SUBJECT TERMS

16. SECURITY CLASSIFICATION OF:			17. LIMITATION OF ABSTRACT	18. NUMBER OF PAGES	19a. NAME OF RESPONSIBLE PERSON
a. REPORT	b. ABSTRACT	c. THIS PAGE			Richard Fernsler
Unclassified	Unclassified	Unclassified	UL	29	19b. TELEPHONE NUMBER *(include area code)* (202) 767-6786

Standard Form 298 (Rev. 8-98)
Prescribed by ANSI Std. Z39.18

CONTENTS

I. Introduction

Producing a plot of collected probe current versus an applied potential sweep (the probe characteristic) is a standard plasma diagnostic technique for determining electron density and temperature in plasmas. After the original work in this area[1], there have been numerous fundamental improvements and inferences from those basic ideas.[2,3] Effectively, the well-known method relies on applying a very low frequency signal to a probe so that both electrons and ions can fully respond to changes in the driving voltage.[4] The dc characteristic, $I_0(V_0)$, depends on probe geometry and is used to find the plasma density via a curve fit, where I_0 is the dc probe current and V_0 the applied voltage with respect to the floating potential. With these definitions, the dc resistance is given by $R_{dc} = V_0/ I_0$. The fitting procedure, either to the electron or the ion saturation portion of the characteristic, has accompanying uncertainties both with respect to probe geometry, and errors associated with the fitting procedure itself. This can render fitting techniques questionable, particularly when probe surfaces become contaminated[5] or when there are two-temperature distributions. Another issue associated with curve fitting is that the electron and ion saturation currents, when used to determine electron density, often produce inconsistent results.[6,7,8] This is an issue yet to be resolved in practical probe data analysis and is also the subject of current investigations at NRL.

Another time-honored method of measuring electron density is based on the rf impedance probe. This technique is based on applying an ac signal which is swept up to and beyond the plasma frequency. A strong resonance occurs at the plasma frequency and, from that resonance, the plasma electron density is readily determined. The applicability of this technique to measurements from space vehicles, where motion of the vehicle can be comparable to thermal ion speeds, was noticed early on[9] and has been employed over the years in a variety of ionospheric measurements. [10,11,12] Temperature is often determined in these cases by using an accompanying Langmuir probe.[12] With these two measurements the Debye length can be obtained and the sheath size estimated.

The rf impedance probe technique developed at the Naval Research Laboratory is useful for a number of reasons[13,14]; one of the most important is the unique determination of the bulk plasma frequency, ω_{pe}, and therefore the electron density. The network analyzer used in these measurments can be calibrated to eliminate cabling impedances and it returns both the real and imaginary parts of the complex impedance from the reflection coefficient.[13] At resonance, the imaginary part of the impedance goes to zero while the real part reaches a peak, indicating maximum transfer of power to the load. These two conditions serve as a dual basis for determining ω_{pe}. The rf measurements are far less sensitive to the effects of surface contamination and secondary electron emission than the conventional voltage sweep analysis.

As another important application of the network analyzer technique, the most recent efforts[14] were concerned with demonstrating the existence of collisionless resistance (CR) in the sheath of a spherical probe when driven by a small rf signal. The CR was shown to be inversely proportional to the plasma density gradient at the location where the applied

Manuscript approved August 7, 2008.

angular frequency equals the electron plasma frequency, ω_{pe} . The expression for the CR derives from a singular integral for the complex plasma impedance and is given by,

$$R(\omega) = \frac{\pi}{2\varepsilon_0 A_r}\left[\frac{d\omega_{pe}}{dr}\right]_{r=r_0} \qquad (1)$$

and is valid for $\omega_{pe}(r_0) < \omega \leq \omega_{pb}$ where $\omega_{pe}(r_0)$ is the plasma frequency at the probe surface, r_0, and ω_{pb} is the bulk plasma density. From this basic expression we are able to construct the sheath density profile by integrating Eq (1) over frequency and inverting. Further details of that work and the origin of Eq. (1) are found elsewhere.[14,15]

The frequency range in this work is applied such that $\omega_{pi} << \omega < \omega_{pe}(r_0)$ where ω_{pi} is the unperturbed ion plasma frequency. The ions are unable to respond to changes in ac voltage but the electrons are. Then, unlike the case where a very low frequency is applied ($\omega < \omega_{pi}$, ω_{pe}), the ac current will have no contribution from the ions. This implies that the ac resistance is only a function of the change in electron current with applied ac voltage. In this region we are able to derive expressions for the electron temperature, the sheath capacitance and the plasma potential. Without an ion response we are effectively including only the electron contribution to the I-V characteristic.

We demonstrate the application of this experimental technique for three small spherical probes for differing environments and plasma conditions. In Section II we describe the theory and assumptions associated with the calculations. In Section III we outline the experimental arrangement in the laboratory and describe the experimental techniques and, in Section IV we compare the values of electron temperature determined using this method with measurements made by a conventional Langmuir probe analysis for each of the spheres.

II. Theory

a. R_{ac} and T_e determination

.

When we apply a small ac voltage to a probe relative to the dc bias, $V_{ac} << V_0$, additional current will flow to the probe. The ac impedance associated with this addition is then $Z_{ac} = V_{ac} / I_{ac}$ and it becomes purely resistive as $\omega \rightarrow 0$. If we let total probe current and voltage be given by $V(t)=V_0+ V_{ac}e^{i\omega t}$ and $I(t)=I_0 + I_{ac}e^{i\omega t}$ and assume, once again, that $V(t)-V_0$ and $I(t)- I_0$ are small, it follows that $Z_{ac} = [V(t)-V_0] / [I(t)- I_0] \approx dV/dI$, where $I(V)$ is the dc probe characteristic. The frequency region of interest for this work involves the range where the ions are not able to respond to the applied signal ($\omega >> \omega_{pi}$); in that case we eliminate ion current contributions and, in the absence of displacement current, total current is carried by the electrons only or $Z_{ac} \approx dV/dI_e$. By avoiding any rf ion current contribution, we are indeed observing dV/dI_e as opposed to dV/dI. In addition, we wish to avoid resonance effects predicted by the earlier collisionless theory and so require that $\omega \leq \omega_{pe}(r_0)$ where r_0 is the probe radius. As already stated, this condition assures that we are investigating the region in frequency space where there is no contribution from the collisionless resonance (*i.e.,* there is a sharp cutoff since the CR

occurs only when the applied frequency is equal to the local plasma frequency; $\omega_{pe}(r_0)$ being the minimum plasma frequency. According to the electron and ion momentum equations, neglecting the ac ion current is justified to order $n_i m_e/n_e M$, where m_e and M are electron and ion masses and n_i is ion density. To a good approximation the electron density obeys the Boltzmann relationship, $n_e(r)=n_0\, e^{\varphi(r)/Te}$ where $\varphi(r) < 0$ is the local potential with respect to the unperturbed plasma and T_e is the electron temperature. Thus, although $n_e << n_i$ near the probe, $\omega_{pi} << \omega_{pe}$ as long as $0 < |V_0/T_e| < 9$ where V_0 is here defined as the dc bias with respect to the plasma. The ac resistance is then given in Gaussian units by,

$$R_{ac} = (dI_e / dV_0)^{-1} = \left(\frac{\lambda_D}{r_0}\right)^2 e^{-eV_0/T_e} \sqrt{\frac{2\pi m_e}{T_e}} \tag{2}$$

provided $\omega_{pi} << \omega \leq \omega_{pe}(r_0)$. In Eq. (2), $I_e(V_0)=4\pi r_0^2 e n_0\, (T_e/2\pi m_e)^{1/2} e^{(eV0/Te)}$ is the dc electron current, and $\lambda_D=(T_e/4\pi e^2 n_0)$ is the electron Debye length. From this expression we may determine the electron temperature by finding R_{ac} at two or more dc voltages in the frequency range indicated. Solving Eq. (1) for T_e,

$$T_e = \frac{e(V_1 - V_2)}{\ln[R_{ac}(V_2)/R_{ac}(V_1)]} \tag{3}$$

We also note in passing that Eq. (2) may be inverted to solve for plasma potential given an independent determination of T_e and n_e. In the work here we have used voltage differences from 1 to 3 V.

b. Circuit model

In order to determine T_e from Eq. (3) we must be able to compute R_{ac} from the network analyzer measurements which provide $Z_{ac}(\omega)$. We consider the plasma as being divided into a quasineutral core plus a non-neutral sheath near the probe. If the rf period is much greater than the time for electrons to cross the sheath, the electrons remain in equilibrium with the total voltage, and therefore $R_{ac} \rightarrow (dI_e/dV)^{-1}$. However there is a capacitance associated with the sheath width which lies in parallel with R_{ac}. The circuit model we use to approximate our probe plasma interface is shown in Figure 1. The primary contribution to the total ac resistance arises from both the real current through R_{ac} and the displacement current through C_s. The net ac sheath impedance becomes,

$$Z_{ac,s}(\omega) = \frac{1}{i\omega C_s + \dfrac{1}{R_{ac} + i\omega L_{sh}}} \tag{4}$$

where L_{sh} is the sheath inductance seen in Fig 1, which we include for completeness and calculate below. We note that C_s will decrease as the dc voltage V_0 is made more negative and the sheath widens.

In treating the region outside the sheath, we assume the plasma is cold and collisionless and that ac current is carried solely by electrons. The ac current density then satisfies $\partial J_{ac}/\partial t = i\omega J_{ac} = e^2 E n_e/m_e$ based on the electron momentum equation. The ac radial electric field is thus given in this region by $E_{ac} = i\omega J_{ac} m_e/e^2 n_e$. The ac voltage drop ΔV_{ac} outside the sheath equals the radial integral of E_{ac} , and since $J_{ac}(r) = I_{ac}/4\pi r^2$ in the absence of sources and sinks, $\Delta V_{ac}/I_{ac} = i\omega L_p$ by definition. With these assumptions the bulk plasma inductance is given by,

$$L_p = \int_{r_s}^{\infty} dr \frac{m_e}{4\pi r^2 e^2 n_e(r)}, \tag{5}$$

Since the sheath region also is characterized by a time-varying electric field induced by the ac signal, the same considerations apply in calculating a sheath inductance or,

$$L_{sh} = \int_{r_0}^{r_s} dr \frac{m_e}{4\pi r^2 e^2 n_{es}(r)}, \tag{6}$$

In these expressions r_s is the sheath radius. The sheath density profile, $n_{es}(r)$, is determined by solving the Poisson equation to determine r_s and the approximate sheath/presheath boundary. The plasma density $n_e(r)$ in the presheath is determined by assuming quasi-neutrality. With these considerations and noting that the plasma inductance is in series with the sheath impedance, the expression for the total ac impedance represented by the circuit of Fig. 1 becomes,

$$Z_{ac}(\omega) = Z_{ac,s}(\omega) + i\omega L_p = \frac{1}{i\omega C_s + \dfrac{1}{R_{ac} + i\omega L_{sh}}} + i\omega L_p \tag{7}$$

or expanding,

$$Z_{ac}(\omega) = \frac{R_{ac}[\omega^2 L_p C_s - 1] + i\omega[\omega^2 C_s L_{sh} L_p - (L_s + L_p)]}{(\omega^2 C_s L_{sh} - 1) - i\omega C_s R_{ac}}. \tag{8}$$

After some algebra we find,

$$\mathrm{Re}(Z_{ac}) = \frac{R_{ac}}{(\omega^2 L_{sh} C_s - 1)^2 + (\omega R_{ac} C_s)^2} \tag{9}$$

and,

$$\mathrm{Im}(Z_{ac}) = \frac{[\omega^3 L_{sh} L_p C_s - \omega(L_{sh} + L_p)](\omega^2 L_{sh} C_s - 1) + \omega R_{ac}^2 C_s(\omega^2 L_p C_s - 1)}{(\omega^2 L_{sh} C_s - 1)^2 + (\omega R_{ac} C_s)^2} \tag{10}$$

We notice from Eq (9) that $Re(Z_{ac})$ is a function of ω whereas R_{ac} as seen in Eq (2) is independent of ω and is a constant for given plasma conditions. Also $Re(Z_{ac})$ becomes purely resistive (= R_{ac}) as $\omega \to 0$.

c. Numerical Algorithm

Since the network analyzer returns $Re(Z_{ac})$ and $Im(Z_{ac})$, and the inductances are calculated based on results of the Poisson equation solution, Eqs (9) and (10) are two equations in the two unknowns, R_{ac} and C_s.

In order to determine the inductances of Eqs. (5) and (6), the Poisson equation is used to construct the density profiles from the spherical surface to pre-sheath. Quasineutrality is then invoked to determine $n_e(r)$ from the pre-sheath edge to infinity. This is accomplished iteratively by specifying the sheath radius as a boundary condition and integrating inward to the sphere bias voltage which will produce that sheath radius for a given plasma density and temperature. Once the bias is determined for a given sheath size, both the sheath and bulk plasma density profiles are known.

The algebra for solving Eqs (9) and (10) is burdensome as they are not easily separable; however, they may be solved numerically. With the solutions for the R_{ac}'s as a function of applied bias and frequency, Eq. (3) may be solved for T_e. We show below these results and comparisons to independent measurements using conventional fitting methods. In the cases below we show results found by sweeping the spherical probes themselves both before and after the frequency runs and applying conventional fitting algorithms which determine density, temperature and plasma potential.[5]

III. Experimental arrangements and technique

Two of the experiments described took place in the large volume portion of the Space Physics experimental facility at the Naval Research Laboratory. This section of the experimental apparatus consists of a cylindrical chamber of diameter 2 m and length 5 m. Argon plasma densities in this work varied in the range of 10^7 to 10^9 cm^{-3}. Typical chamber pressure was 1×10^{-4} Torr. A typical electron-neutral collision frequency for these plasmas is $\nu_{en} \sim 6 \times 10^5$ s^{-1} which is much less than the plasma frequency, $\omega_{p0} \sim 6 \times 10^8$ s^{-1} ($f_{p0} \sim 100$ MHz). Neutrals and ions are at room temperature. The plasma is created by a recently-redesigned tungsten filament source biased to near -70 Volts and covering a large portion of the inner end-plate surface area. A low-level axial magnetic field on the order of 1-2 Gauss is provided by 5 circular water-cooled coils aligned axially in a Helmholtz configuration; magnetic field strengths near 1 kG are available for other experimental programs. Some of the experiments done here were done without an external field. Electron density and temperature measurements are typically done with a cylindrical Langmuir probe which is constantly heated to prevent contamination buildup[5] or with an emissive probe. Further details of the experimental configuration and the general laboratory setup for different configurations are to be found elsewhere.[13,14]

The other experiment covered here took place in a smaller chamber originally designed and used for dusty plasma experimentation. The DUsty PLasma EXperiment (DUPLEX) chamber is a transparent polycarbonate cylindrical vacuum chamber which is 46 cm in diameter and 61 cm in height.[16] The experimental volume can be accessed from the top by an aluminum plate with five vacuum flanges. The cylinder rests on a

stainless steel chamber plate through which access is provided to a 4-in diffusion pump-based vacuum system. At the bottom of this chamber, separated by approximately 50 cm from the spherical impedance probe used in these studies, is a biased filament DC discharge source which produced an argon plasma with a typical density near 10^8 cm^{-3} at a pressure $0.1 < P_N < 0.5$ mTorr. The biased discharge source voltage is in the range of about -50 to -70 Volts. The base pressure is near .01 mTorr. The impedance probe is cleaned between runs by heating with a high power (~ 200 W), retractable lamp which is in close proximity during the cleaning process and retracted during experimentation. Experiments done in this facility used exclusively the 3 mm radius sphere. The plasma environment was characterized typically by higher electron temperatures than in the large chamber environment.

Three small stainless steel spheres of 3 mm, 9.5 mm and 12.5 mm radius were connected to an HP8735D Network Analyzer through 50 Ω coaxial cable for the data presented in this work. The 9.5 and 12.5 mm spheres were mounted on a 1/4 inch diameter ceramic and steel support which is connected to 1/4 inch diameter semi-rigid copper 50 Ohm coaxial cable. This improvement over previous versions of this diagnostic[11] was made so that the probes could withstand much higher temperatures while being sputter cleaned. Primary cleaning of the 3 mm probe was accomplished with a retractable heat lamp as described above.

For all of the experiments, the determination of plasma impedance depends upon the network analyzer measurement of the complex reflection coefficient, $\Gamma(\omega)$. From this measurement the analyzer returns as separate outputs *Re* $Z_{ac}(\omega)$ and *Im* $Z_{ac}(\omega)$ where,

$$Z_{ac}(\omega) = Z_0[\frac{1+\Gamma(\omega)}{1-\Gamma(\omega)}] \tag{13}$$

and Z_0 (=50 Ω) is the internal impedance of the analyzer. We also note that the ratio of reflected-to-total power is given by,

$$|\Gamma|^2 = \frac{P_r}{P_0} \tag{14}$$

where $P_0 = P_R + P_T$ with P_R and P_T the reflected and transmitted powers, respectively. (The quantity $1-|\Gamma|^2$ is the normalized transmitted power and this output is also available). The impedance from the cabling and support is compensated through instrument calibration when connected to a 50 Ω resistor or when calibrated as an open, or short, circuit. An open circuit corresponds then to Γ=1, a short circuit to Γ=-1 and if the load impedance is a perfect match, Γ=0. As the change in the complex reflection coefficient for the sphere in the plasma is very small, this calibration is a critical step. Care must be taken to avoid unwanted rf noise or reflections from the chamber walls or other nearby probes. The method is tested by connecting other known resistances and capacitances to the end of the probe shaft to ensure that any error is much smaller than the changes in the impedance we wish to measure. These considerations are covered in more detail elsewhere.[13]

IV. Experimental Results and Temperature Measurement Comparisons

a. Applied bias levels and frequency range considerations

When applying Eq. (3) to find T_e for an argon plasma, it can be shown that biases could range as high as about -9 Volts for a 1 eV plasma. That, however, is not the primary limiting factor in this case. The bias levels applied to the probe for the purpose of calculating temperature as indicated in Eq. (2) typically ranged from 0 to -3 Volts in steps of 1 Volt. The restriction on applicable bias levels is demonstrated in Fig. 2 which derives from the Boltzmann approximation, which allows us to express the electron plasma frequency at the probe as,

$$\omega_{pe}(r_0) \simeq \omega_{pi} e^{-\Delta V/2T_e} \sqrt{\frac{M}{m_e}} \qquad (15)$$

where T_e is the electron temperature, M is ion mass and ω_{pi} is the ion plasma frequency. In this expression ΔV is the applied bias with respect to plasma potential. Here, and throughout the paper, we stress that we only consider biases less than the plasma potential. The restrictions both on applicable bias levels and frequency range information of Eq. (15) can be inferred from Fig. 2. These data were taken with the 0.95 cm radius probe in the large vacuum chamber where for this run $n_{e0} = 2.3 \times 10^8$ cm^{-3} and the plasma potential was +1.9 Volt. We use an approximate T_e found from conventional analysis in plotting Eq. (15). The figure indicates decreasing plasma frequency (electron density) at the probe surface for increasing (negative) bias as would be expected. From the figure, it is clear that for a bias level of $\Delta V = -3$ V, the frequency range used to find T_e is restricted to less than about 23 MHz. Since for this argon plasma, the ion plasma frequency, f_{pi}, is near 0.5 MHz, we are restricted to a fairly narrow range of available frequencies (i.e., $\omega_{pi} << \omega \leq \omega_{pe}(r_0)$). For comparison, the bulk electron plasma frequency is about 136 MHz. For biases more negative than -3 V, the frequency ranges become too narrow to get a sufficient representation of R_{ac} (which is not a function of ω) and hence a solution to Eq. (3) becomes more difficult. Further, the curve of Fig. 2 serves to delineate the cutoff frequency for the collisionless resistance model; for a given sphere bias there will be no contribution of collisionless resistance to the net ac impedance for any lower frequency than that at the given bias in the figure. At higher frequencies the net impedance will contain contributions from the collsionless resistance as well as from the lower frequency impedance treated in this paper.

b. Data and determination of T_e

The first data set we analyze is based on the 3 mm radius stainless steel sphere in the DUPLEX chamber described above. We demonstrate in graphical form the construction method for determining T_e from the data taken by the network analyzer. For a portion of the later data using different spheres of varying diameter in a larger chamber, we show

only the results of the measurements along with comparisons to determination of T_e by standard fitting routines used with the spheres operated as conventional Langmuir probes.

Plotted in Fig. 3 is the comparable plot to Fig. 2 for the 3mm probe data. From comparison of the two plots one can see the strong impact of T_e on the allowed frequencies before cut-off. *i.e.,* whereas in Fig. 2 for $T_e \sim 1$ eV, a voltage bias of -4 Volts places the cutoff at near 14 MHz, in the case of Fig. 3 at a comparable density but at $T_e \sim 3$ eV, it is not possible to analyze the data to determine T_e at this bias. Even for a bias of -3 Volts the frequency range allowable is severely restricted *i.e.*, $f_{pi} \sim 0.6$ MHz and $f_{pe}(r_0) \sim 1.8$ MHz. Therefore for this temperature and density we are restricted to biases no larger than ~ -3 Volts.

Fig. 4 is a plot of $Re(Z_{ac})$ versus frequency for probe biases varying from 0 to -4 volts for the 3 mm radius sphere. This example shows the frequency dependence of the function as seen in Eq. (9). We contrast this to Fig. 5 where the results for R_{ac} vs applied frequency are plotted. R_{ac} is averaged over the frequency ranges and this mean value, for a given applied bias, is plotted as a straight line and used to determine T_e using Eq. (3). Fig. 6 shows T_e versus the voltage range bin chosen, along with the mean value (black solid line) and the value of T_e determined by our Langmuir probe fitting routines (red solid line). As an example if we select voltage bins which include voltages varying from 0 to -3 Volts in steps of 1 V, this allows 6 different calculations of T_e corresponding to the voltage bins: (1) 0,-1 V ;(2) 0,-2 V; (3) 0,-3V; (4) -1,-2V; (5) -1,-3V; and (6) -2,-3V. In the case of Fig. 5 we have included biases from 0 to -3 Volts even though the final voltage bin 6 (-2,-3 V) is again restricted in the number of usable frequencies according to Fig 3.

The results for the 9.5 mm probe in the large plasma chamber environment described above are seen in Figs. 7 and 8 for B=0 and in Figs 9 and 10 for B=1 Gauss. Figs 11 and 12 show only T_e for the 12.5 mm radius probe under conditions differing only slightly in T_e and n_e

As a final example we show a data set taken for the 12.5 mm probe at low density ($n_e \approx 1.2 \times 10^7$ cm-3) and higher temperature (Te ≈ 2.6 eV) using an He plasma. The plasma potential is near 3.8 Volts. Because of the low electron density we are again restricted in terms of the frequency range in order not to include any contribution from the resonant CR as covered above. The biases vary only from 0 to -2 V. The cutoff frequency is near 10 MHz but we further restrict that frequency to 6 MHz to be safely below this range. Instead of using a value of R_{ac} which is averaged over the available frequency ranges as in the earlier plots, here we plot T_e vs applied frequency for each of the bias voltage ranges separately in Fig. 13. The plot shows 3 values for each frequency applied corresponding to the voltage bins for a 0 to -2 Volt range. As in the data above the standard deviation is taken for the points about the mean value of calculated (theoretical) temperature.

V. Summary

We have introduced a method of determining electron temperature for small spherical probes using results of a network analyzer determination of impedance. The method does not depend on fitting routines and hence does not require a specific form to be used while interpreting an I-V characteristic. However, it does require estimates for L_{sh}, L_p and C_s. The method is robust in the sense that it not affected by probe contamination and does not formally depend upon the assumption of a single Maxwellian distribution. Finally, the number of independent determinations of T_e can be increased by using finer resolution voltage bins than we have used in this work.

As can be seen in the comparisons above, temperatures obtained by the method tend to differ, in some cases more and some less, from those determined by a fit using conventional analysis. Generally the temperatures in the large chamber using the new method are higher than those produced by the conventional fitting procedures. We plot in Fig. 14 the values for Te determined by the different methods in this paper versus each other. Although it is clear that generally the temperatures measured by the impedance method outlined here are higher, the agreement appears reasonable between the two methods. One possible source of error in conventional I-V analysis involves the ion contribution to the total current, particularly for negative bias levels. For example, the existence of a small component of thermalized hot electrons can have a major effect on the determination of ion current in the ion saturation region. This holds true if a two-temperature distribution is present and not accounted for. If, due to the presence of the small hot electron component, the ion saturation current is estimated to be smaller than it actually is, this can influence the calculation of the bulk plasma temperature depending on the particular analysis method employed. In a recent work[17], we show that a surprisingly small component of higher temperature can have a dramatic effect on ion saturation current determination.

VI. Figure Captions

Figure (1) – Circuit schematic analogy to probe/sheath/plasma used to estimate impedance.

Figure (2) – Plasma frequency at the probe surface, $f_{pe}(r_0)$, vs applied bias voltage, V_{bias}, wrt to plasma potential, V_{plasma}. N_e = 2.3 x 10^8 cm^{-3} , r_0 = .95 cm

Figure (3) - Plasma frequency at the probe surface, $f_{pe}(r_0)$, vs applied bias voltage, V_{bias}, wrt to plasma potential, V_{plasma}. N_e = 5.3 x 10^8 cm^{-3} , r_0 = .33 cm

Figure (4) – $Re(Z_{ac})$ vs frequency for 5 different bias voltages. N_e = 5.3 x 10^8 cm^{-3} , r_0 = .33 cm

Figure (5) – R_{ac} vs frequency and averages for 4 different biases. (V=0, black;V=-1, red;V=-2;green; V=-3 blue) N_e = 5.3 x 10^8 cm^{-3} , r_0 = .33 cm

Figure (6) – T_e fit (red) and T_e average (black) vs bias voltage range bin: (1) 0,-1 V (2) 0,-2 V, (3) 0,-3 V (4) -1, -2 V (5) -1,-3 V (6) -2,-3 V. Te(average)(black) = 2.63 eV, σ = 0.426 eV N_e = 5.3 x 10^8 cm^3 r_0 = .33 cm.

Figure (7) – R_{ac} vs frequency and averages for 4 different biases. (V=0, black;V=-1, red;V=-2;green; V=-3 blue) . N_e = 2.3 x 10^8 cm^{-3} , r_0 = .95 cm

Figure (8) – T_e fit (red) and T_e average (black) vs bias voltage range bin: (1) -1,-2 V (2) -1,-3 V, (3) -1,-4 V (4) -2,-3 V (5) -2,-4 V (6) -3,-4 V. Te(average) = 0.73 eV, σ = 0.11 eV, N_e = 2.3 x 10^8 cm^3 r_0 = .95 cm.

Figure (9) – R_{ac} vs frequency and averages for 4 different biases. (V=0, black;V=-1, red;V=-2;green; V=-3 blue) . N_e = 3.38 x 10^8 cm^{-3} , r_0 = .95 cm, B = 1 Gauss

Figure (10) – T_e fit (red) and T_e average (black) vs bias voltage range bin: (1) -1,-2 V (2) -1,-3 V, (3) -1,-4 V (4) -2,-3 V (5) -2,-4 V (6) -3,-4 V. Te(average) = 1.06 eV, σ = 0.17 eV, N_e = 3.38 x 10^8 cm^3 r_0 = .95 cm. B = 1 Gauss

Figure (11) - T_e fit (red) and T_e average (black) vs bias voltage range bin: (1) 0,-1 V (2) 0,-2 V, (3) 0,-3 V (4) -1, -2 V (5) -1,-3 V (6) -2,-3 V. Te(average) = 1.85 eV, σ = 0.076 eV N_e = 5.2 x 10^7 cm^3 r_0 = 1.25 cm.

Figure (12) - T_e fit (red) and T_e average (black) vs bias voltage range bin: (1) 0,-1 V (2) 0,-2 V, (3) 0,-3 V (4) -1, -2 V (5) -1,-3 V (6) -2,-3 V. Te(average) = 1.59 eV, σ = 0.12 eV N_e = 3.6 x 10^7 cm^3 r_0 = 1.25 cm.

Figure (13) - T_e fit (red) and T_e average (black) vs frequency and averages for 5 different biases. σ = .18 eV, Te(average) = 2.59 eV, N_e = 1.27 x 10^7 cm^{-3} , r_0 = 1.25 cm, B = 1 Gauss

Figure (14) – Te fit vs Te (impedance) for 6 different experimental series.

VII. References

[1]I. Langmuir and H. Mott-Smith, Gen. Elec. Rev., **27**, 449, 538, 616, 762 (1924)

[2]F.F. Chen, *Plasma Diagnostic Techniques* (Academic, San Diego, CA, 1965)p. 113ff

[3]J.G. Laframboise, UTIAS Rpt. **100** (1966)

[4]F.W. Crawford and R.F. Mlodnosky, J. Geophys. Res., **69**, 2765 (1964)

[5]W.E. Amatucci, P.W. Schuck, D.N. Walker, P.M. Kintner, S. Powell, B. Holback, and D. Leonhardt, Rev. Sci. Instrum., **72**, 2052 (2001)

[6]D. Lee and N. Hershkowitz, Phys. Plasmas, **14**, 033507 (2007)

[7]B.M Annaratone, M.W. Allen and J.E. Allen, J. Phys. D:Appl. Phys, **25**, 417 (1992)

[8]F.F. Chen, C. Etievant and D Mosher, Phys. Fluids, **11**, 811 (1968)

[9]J.E. Jackson and J.A. Kane, J. Geophys. Res. **64**, 1074 (1959)

[10]M.A. Abdu, P. Muralkrishna, I.S. Batista, and J.H.A. Sobral, J. Geophys. Res. 96, 7689 (1991)

[11]M.D. Jensen and K.D. Baker, J. Spacecr. Rockets **29**, 91 (1992)

[12]C.T. Steiges, D. Block, M. Hirt, B Hipp, A. Piel and J Grygorczuk, J. Phys. D:Appl. Phys. **33**, 405 (2000)

[13]D.D. Blackwell, D.N. Walker, and W.E. Amatucci, Rev. Sci. Instrum.**76**,023503 (2005); D.D. Blackwell, D.N. Walker, S.J. Messer, W.E. Amatucci, Phys. Plasmas **12**, 093510 (2005)

[14]D.N. Walker, R.F. Fernsler, D.D. Blackwell, W.E. Amatucci, and S.J. Messer, Phys. Plasmas **13**, 032108 (2006)

[15]D.N. Walker,R.F. Fernsler, D.D. Blackwell, and W.E. Amatucci, NRL Memorandum Report, **6750-07-9033** (2007)

[16]W.E. Amatucci, D.N. Walker, George Gatling, and E.E. Scime, Phys. Plasmas **11**, 2097 (2004)

[17]R.F. Fernsler, *Plasma Sources Science and Technology*, (accepted (8/2008)

VIII. Figures

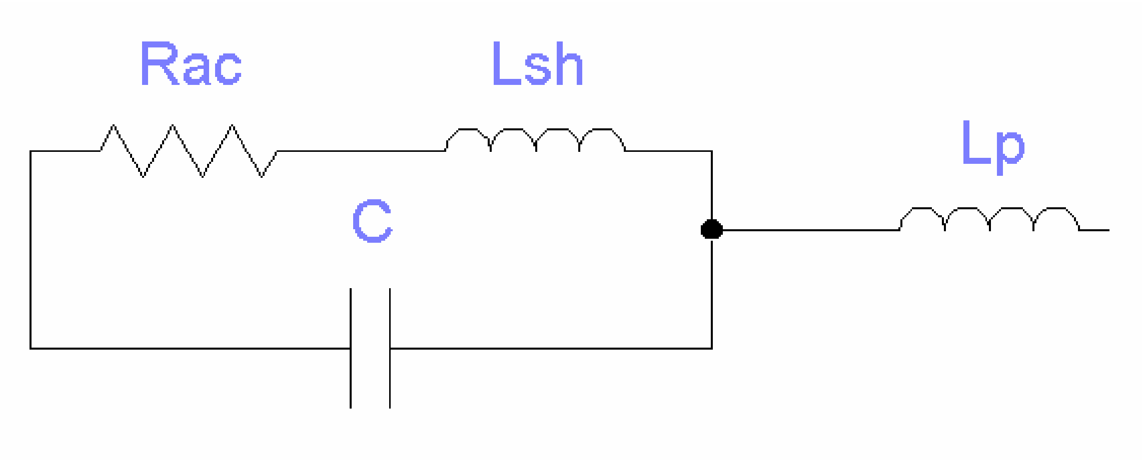

Figure 1

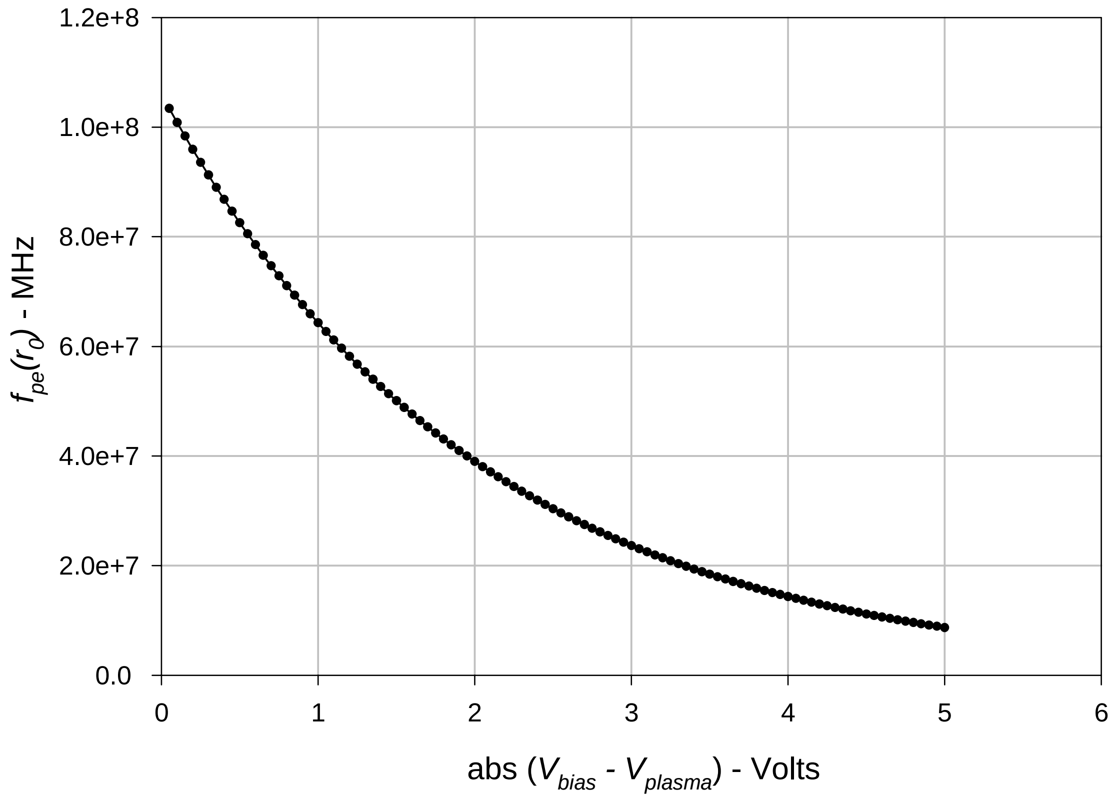
1.2e+8
1.0e+8
8.0e+7
6.0e+7
4.0e+7
2.0e+7
0.0
0
1
2
3
4
5
6
$f_{pe}(r_0)$ - MHz
abs (V_{bias} - V_{plasma}) - Volts

Figure 2

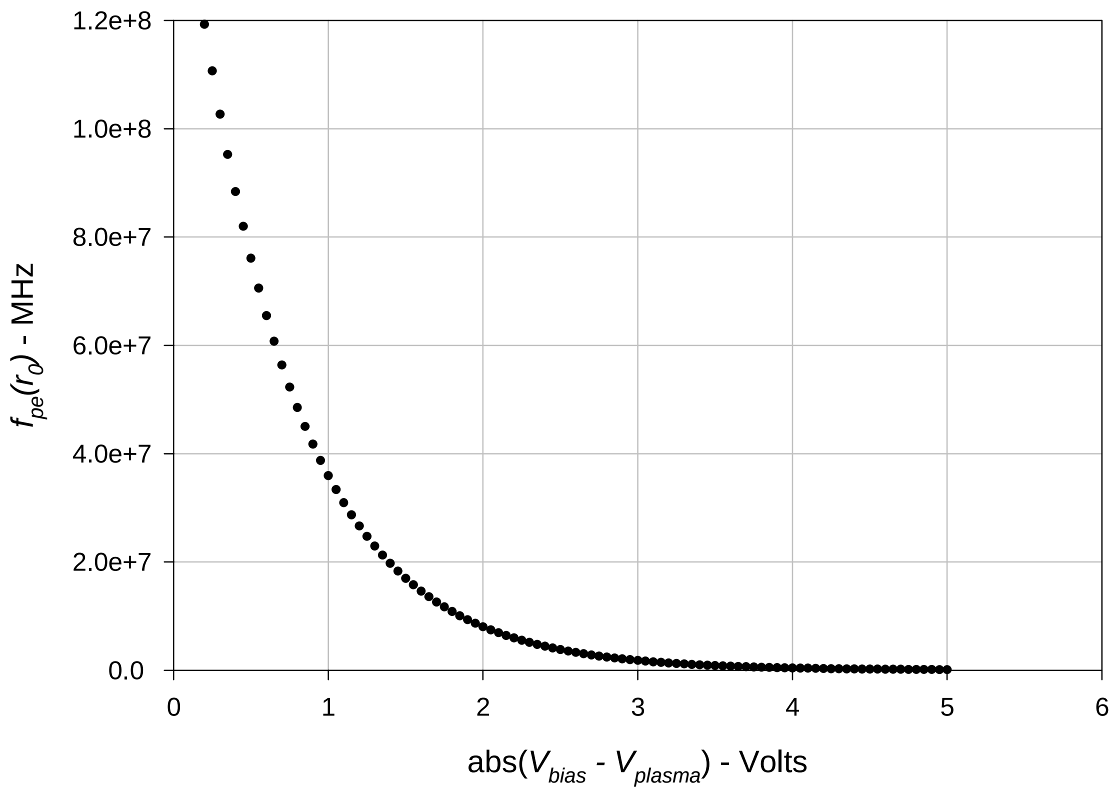
1.2e+8
1.0e+8
8.0e+7
6.0e+7
4.0e+7
2.0e+7
0.0
0
1
2
3
4
5
6
$f_{pe}(r_0)$ - MHz
abs(V_{bias} - V_{plasma}) - Volts

Figure 3

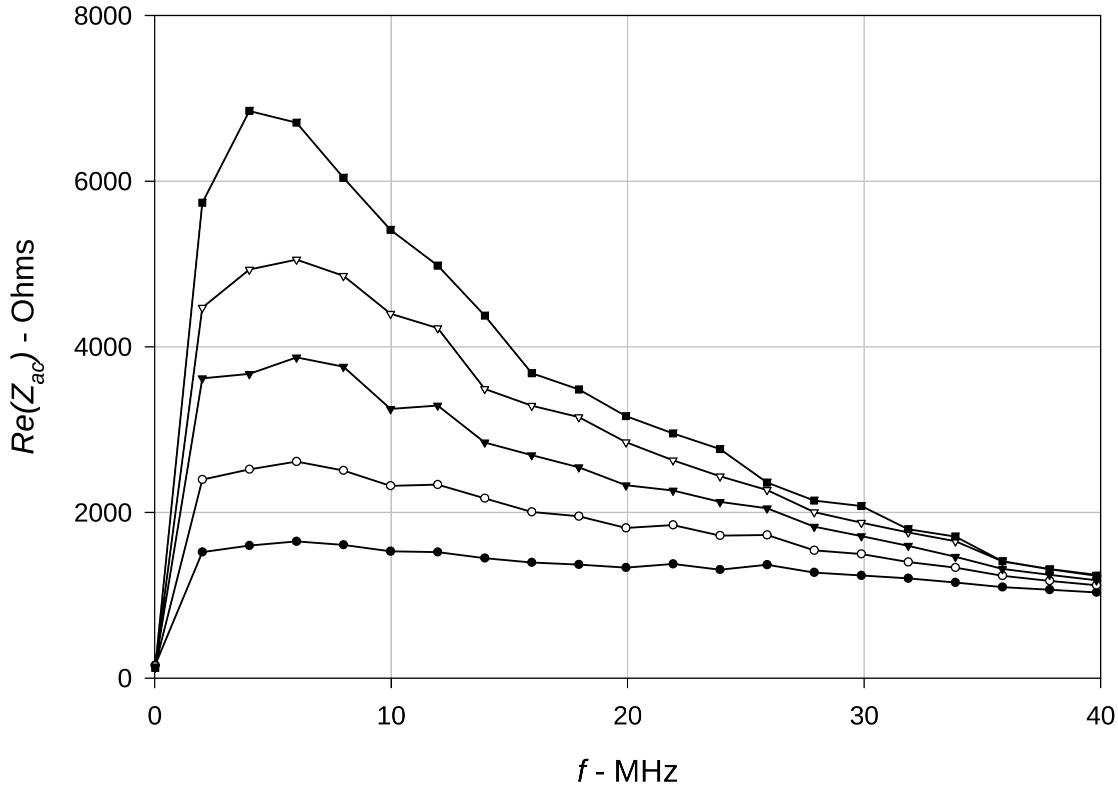

Figure 4

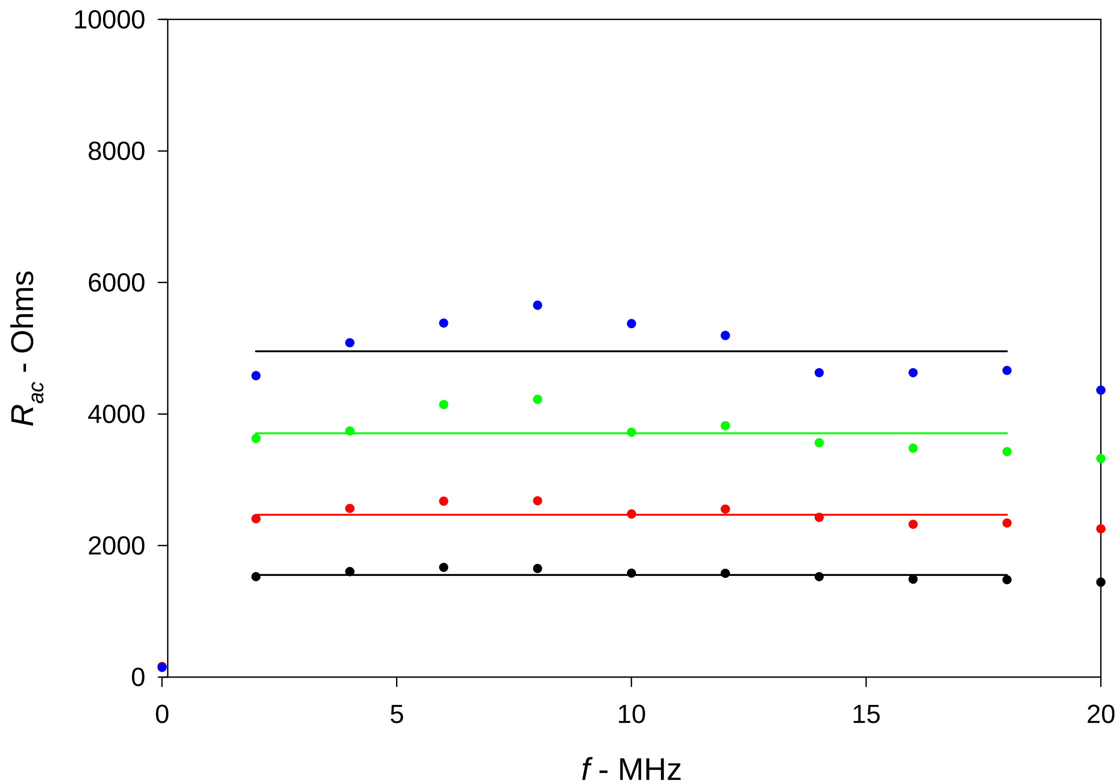

Figure 5

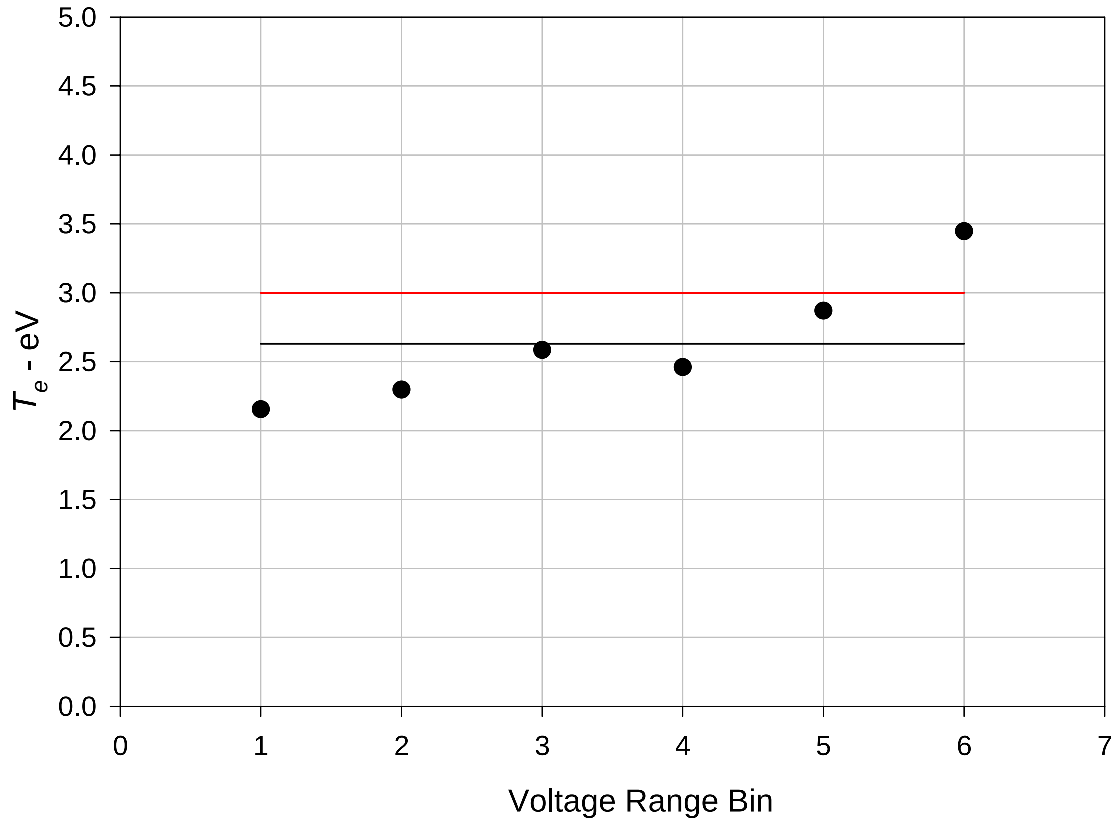

Figure 6

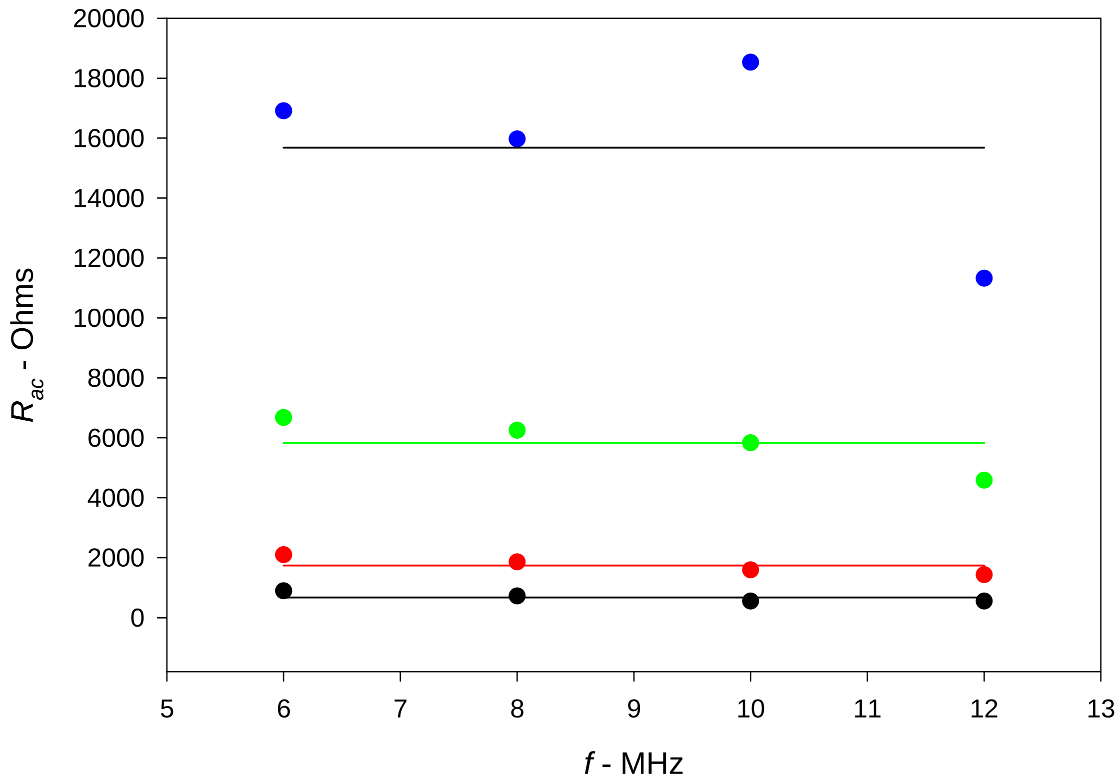

20000
18000
16000
14000
12000
10000
8000
6000
4000
2000
0
R_{ac} - Ohms
5
6
7
8
9
10
11
12
13
f - MHz

Figure 7

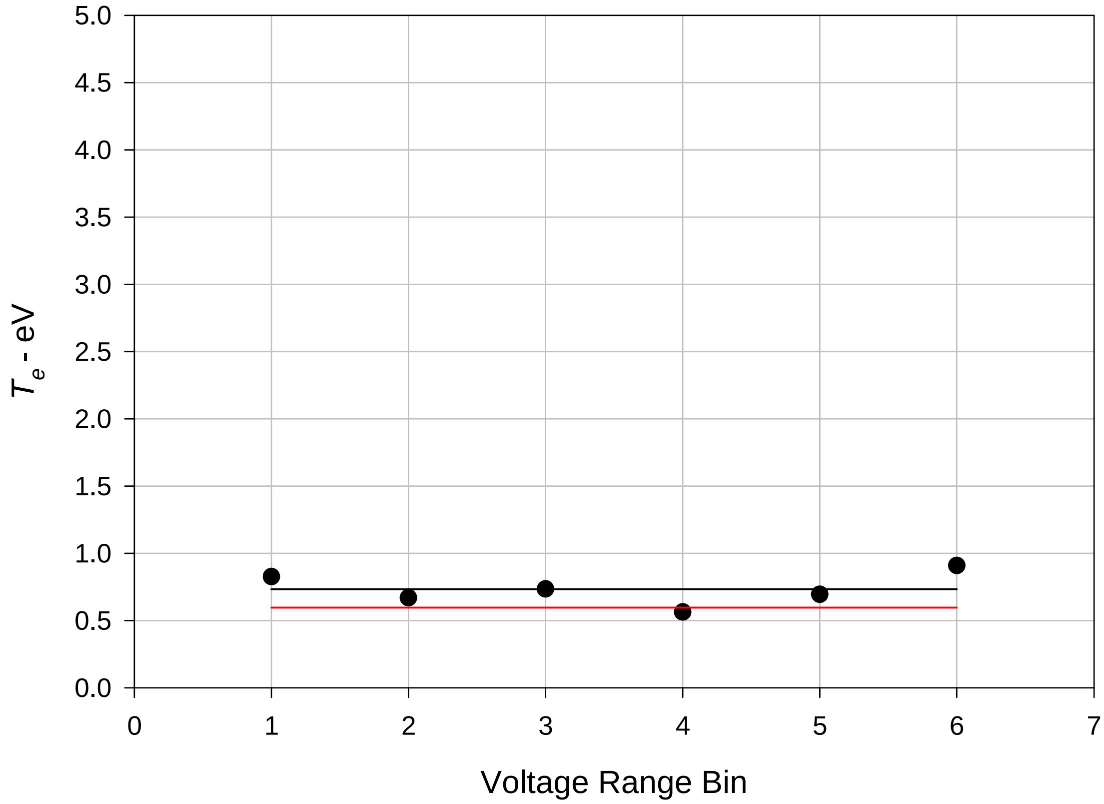

Figure 8

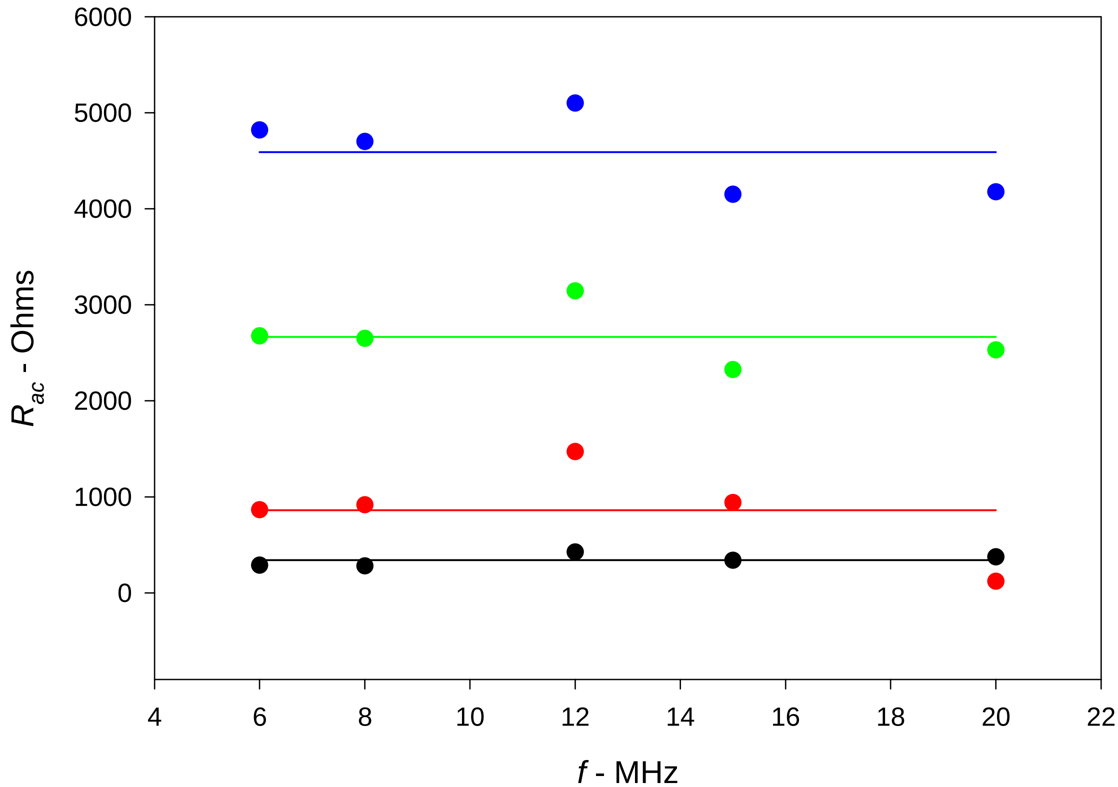
6000
5000
4000
3000
2000
1000
0
R_{ac} - Ohms
4
6
8
10
12
14
16
18
20
22
f - MHz

Figure 9

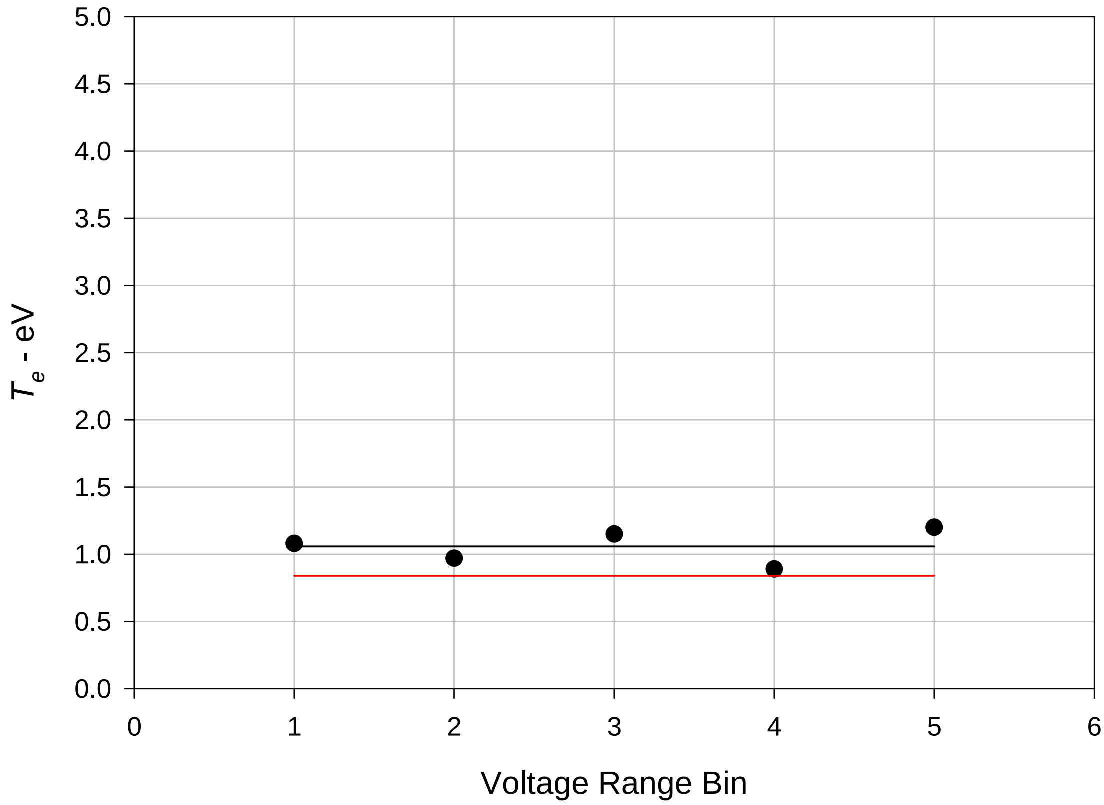

Figure 10

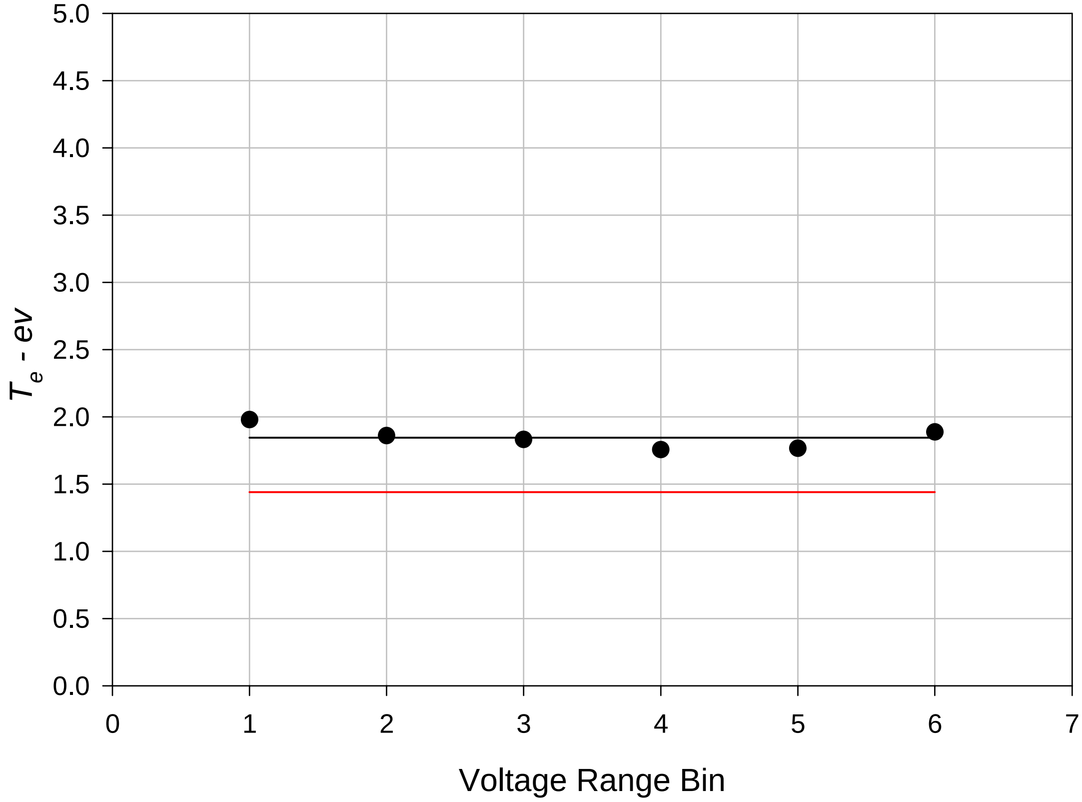

Figure 11

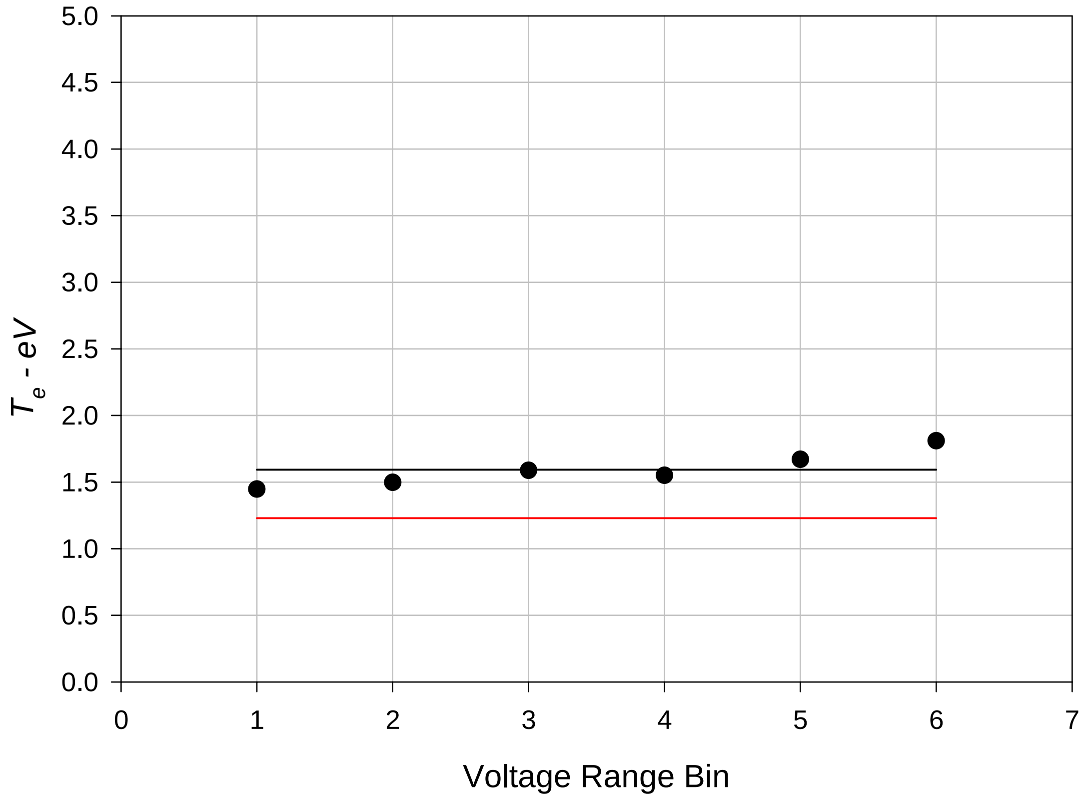

Figure 12

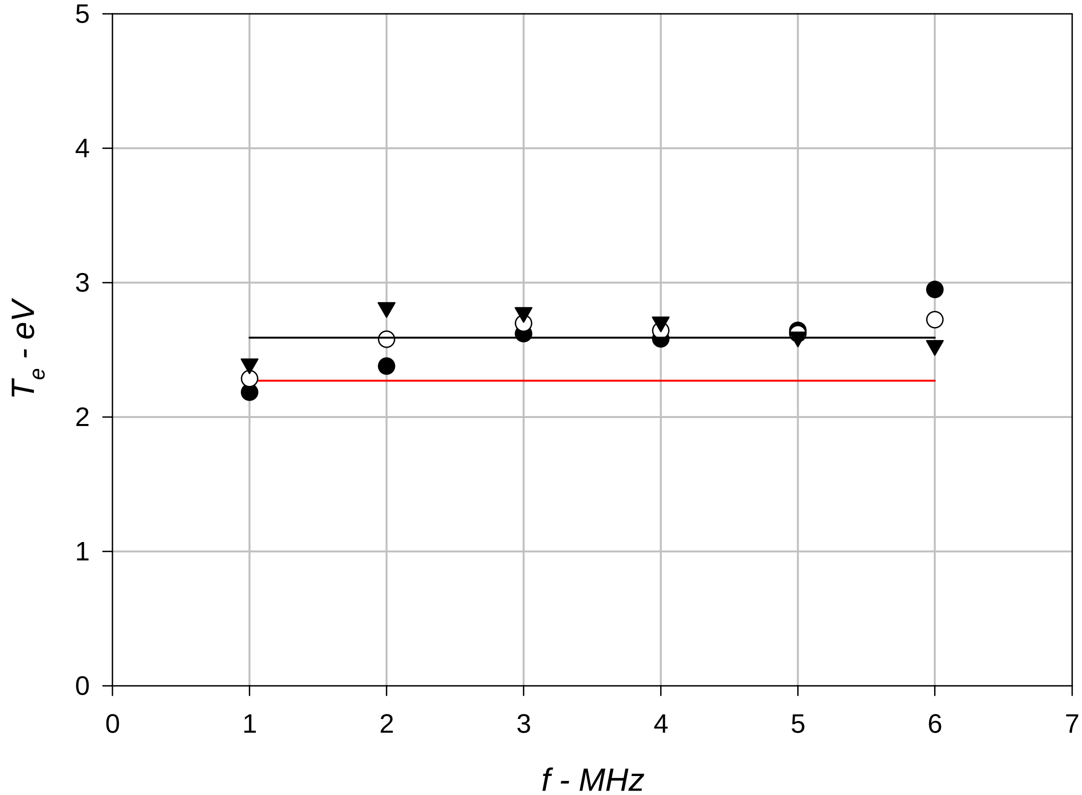

Figure 13

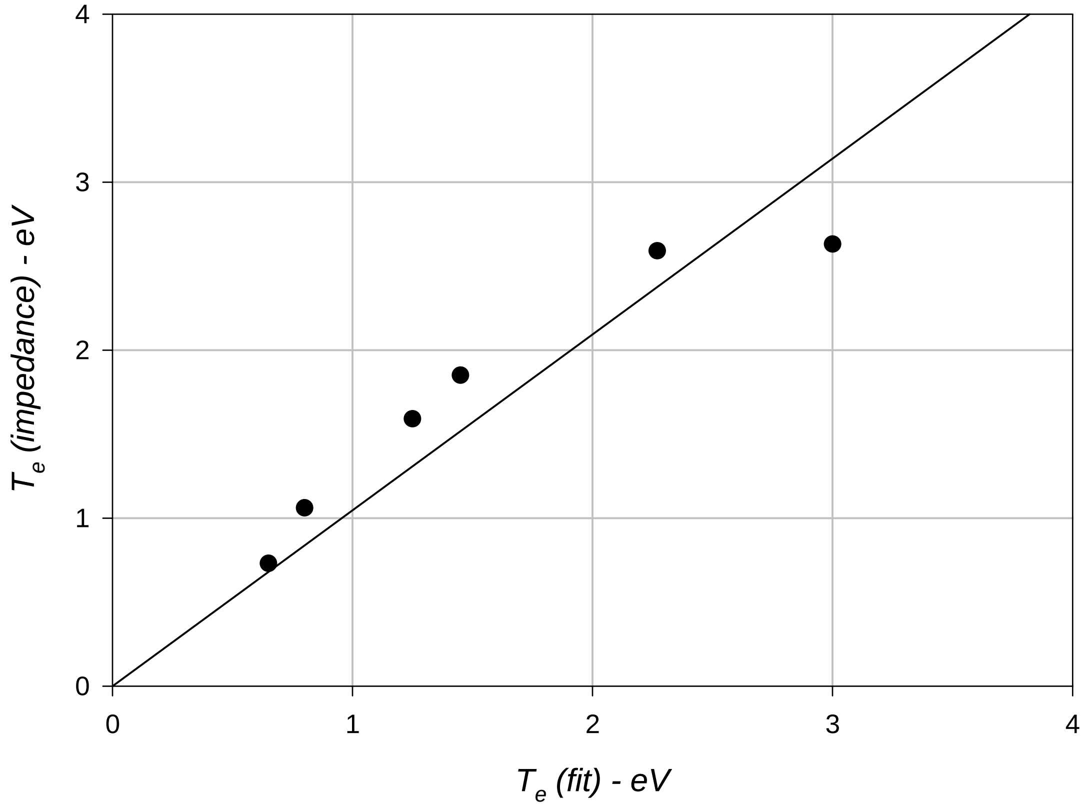

Figure 14